Engineering Structures 179 (2019) 92–105

Contents lists available at ScienceDirect

Engineering Structures

journal homepage: www.elsevier.com/locate/engstruct

An efficient framework for the inelastic performance assessment of structural systems subject to stochastic wind loads

Wei-Chu Chuang, Seymour M.J. Spence*

Department of Civil and Environmental Engineering, University of Michigan, Ann Arbor, MI 48109, USA

ARTICLE INFO

Keywords:
Inelastic wind response
Dynamic shakedown
Performance-based wind engineering
Stochastic wind loads
Monte Carlo simulation

ABSTRACT

The modeling and estimation of the inelastic response of wind excited structures is attracting growing interest with the introduction of performance-based wind engineering. While frameworks based on direct integration have been widely adopted in earthquake engineering for estimating inelastic responses, the significantly longer duration of typical windstorms, as compared to seismic events, makes this approach extremely computationally challenging in the case of wind excited systems. This is especially true in the case of modern performance-based wind engineering frameworks, which are based on probabilistic metrics estimated through simulation and therefore repeated evaluation of the system. This paper addresses this challenge through the development of a simulation framework based on dynamic shakedown theory. In particular, an efficient path-following algorithm is proposed for estimating not only the shakedown multipliers, but also the plastic strains and deformations associated with occurrence of the state of shakedown. The efficiency with which this information can be estimated for any given wind load time history enables the development of a simulation-based framework, driven by general stochastic wind load models, for the estimation of the system-level inelastic performance of the structure. The validity and practicality of the proposed framework is illustrated on a large-scale case study.

1. Introduction

With the introduction of performance-based design (PBD) frameworks in wind engineering, inelastic/non-linear performance assessment is assuming an increasingly important role. Indeed, PBD approaches require the evaluation of building performance under various hazard levels, including structural behavior beyond the elastic limit. In seismic engineering, many methods have been developed for characterizing the inelastic behavior of the structure based on direct step-by-step integration [1], including specialized methods such as incremental dynamic analysis (IDA) [2]. In the field of wind engineering, however, the extremely long duration of typical windstorms effectively prevents the application of such computationally intensive methods, as they require non-linear dynamic integration over the entire load history. This computational hurdle becomes exasperated in applying modern performance-based wind engineering frameworks that are based on propagating uncertainty through the system using simulation methods that require the repeated evaluation of the system [3–9]. Notwithstanding these issues, a number of studies have been carried out over the years using direct integration methods with the aim of better understanding the inelastic behavior of wind excited systems [10–15]. These studies have provided insight into the inelastic failure mechanisms affecting wind excited structures, e.g. ratcheting in the alongwind direction and low cycle fatigue in the acrosswind direction. In alternative to direct integration, methods have recently been proposed based on nonlinear static pushover analysis [16]. While providing significant computational gains over direct integration, these methods are affected by the inherent difficulty of nonlinear static pushover analysis to capture cumulative damage mechanisms, e.g. ratcheting and low cycle fatigue [17,18]. This has led to the recent development of a computationally efficient approach for determining safety of wind excited systems against these inelastic failure mechanisms within the context of simulation-based wind PBD frameworks [19,9]. This approach is based on applying the theory of dynamic shakedown [20–24] as a means to rapidly provide a complete picture of the inelastic structural behavior, from incremental plastic collapse to low cycle fatigue. Based on the extension of the classic Bleich-Melan and Koiter shakedown theorems [25] to dynamic excitation, this approach was developed to determine if an elastoplastic structure subject to a given dynamic load history will eventually respond elastically after a finite amount of plastic deformation. While theoretical frameworks for dynamic shakedown of systems subject to excitation of finite duration have been proposed [23,24], a special case that significantly facilitates the determination of the state of dynamic shakedown exists

* Corresponding author.
E-mail addresses: wechuang@umich.edu (W.-C. Chuang), smjs@umich.edu (S.M.J. Spence).

https://doi.org/10.1016/j.engstruct.2018.10.039
Received 10 February 2018; Received in revised form 25 July 2018; Accepted 16 October 2018

when the external loads can be considered of infinite duration and periodic. This special case is at the basis of the approaches outlined in [19,9] where the finite duration of real dynamic wind loads was considered by simply repeating indefinitely the windstorm of interest. In particular, if the yield domains of the structure are modeled as piecewise linear, the limit state that separates plastic collapse from the safe state of dynamic shakedown can be efficiently identified through solving a linear programming problem (LPP) for each dynamic wind load trace of interest [19]. The efficacy with which LPP problems can be solved in high dimensions has enabled this approach to be integrated in simulation-based wind PBD frameworks applied to large-scale structural systems [9].

Notwithstanding these advances, a significant limitation of the approaches outlined in [19,9] is the lack of any estimation of the plastic deformations and strains that occur during the process of dynamic shakedown. This limits the applicability of these approaches, as these quantities play a fundamental role in determining whether a building is repairable after an extreme wind event, or, more critically, if the building has collapsed due to asymptotically limited but excessive plastic deformations. To overcome this limitation, this paper is focused on the development of models for the efficient estimation of the plastic deformations and strains occurring during shakedown under a given dynamic wind load time history. By integrating these approaches with data-driven stochastic models for describing the record-to-record variability of the dynamic wind load histories, a Monte Carlo framework is proposed for rapidly assessing the collapse performance of large-scale wind excited systems within recently introduced probabilistic performance-based wind engineering frameworks.

2. Problem setting

The Pacific Earthquake Engineering Research (PEER) Center's framework for performance-based earthquake engineering [26–28] was recently extended to wind engineering [3,29,9]. In particular, within an intensity-based assessment setting, this framework measures performance in terms of the following conditional exceedance probability:

$$P_f(dv|im) = \iiint G(dv|dm)\cdot|dG(dm|edp)|\cdot|dG(edp|ip)|\cdot|dG(ip|im)| \tag{1}$$

where dv is a decision variable threshold of interest (e.g. critical repair cost or downtime value); $G(a|b)$ is the complementary cumulative distribution function of a conditional on b; dm is the damage measure; edp is the engineering demand parameter, which for structurally induced damage is generally taken as the peak structural response over the duration of the wind event; ip represent interaction parameters (i.e. the stochastic aerodynamic loads acting on the structure); while im is the intensity measure which, in the case of wind hazards, is generally taken as a wind speed with specified mean recurrence interval (MRI).

As pointed out in [9], strictly speaking, the framework of Eq. (1) only applies to buildings that are repairable, i.e. those that do not collapse during the windstorm of intensity im. To further consider both collapse and non-collapse scenarios, the following decomposition based on the total probability theorem can be used:

$$\begin{aligned} P(DV > dv|im) = {} & P(DV > dv|NC, im)P(NC|im) \\ & + P(DV > dv|C, im)P(C|im) \end{aligned} \tag{2}$$

where $P(C|im)$ and $P(NC|im)$ are the conditional probability of collapse and non-collapse for the wind event of intensity im, $P(DV > dv|NC, im)$ is the exceedance probability of dv given that the building does not collapse (i.e. the contribution to $P(DV > dv|im)$ of Eq. (1)), while $P(DV > dv|C, im)$ is the exceedance probability of dv given that the building collapses during the wind event of intensity im. In general, a wind excited structure can be identified as collapsed under two possible failure scenarios: (1) failure due to low cycle fatigue (acrosswind failure) or incremental plastic collapse (alongwind failure); and (2) failure due to excessive plastic deformations and strains, e.g. excessive peak/residual displacements or hinge rotations. In order to estimate the collapse and non-collapse probability associated with the first failure scenario, dynamic shakedown theory can be applied to define a limit state separating low cycle fatigue and/or incremental plastic collapse from the safe state of dynamic shakedown [19]. This method, however, does not provide any information on the plastic strains and deformations of the structure, which are essential for not only evaluating the second collapse scenario, but also for estimating $P(DV > dv|NC, im)$ in the case of non-collapse. This paper is focused on developing models that address this issue therefore enabling a general description of failure.

Before closing this section, it should be observed that Eq. (2) provides a general framework that can be used to assess a set of performance objectives, ranging from serviceability to collapse prevention, by identifying for each performance objective a value of interest for the intensity measure (e.g. a wind speed with an MRI of interest) and an appropriate decision variable.

3. Mechanical model

For a given external dynamic wind load, the inelastic response of the structural skeletal systems of interest to this work can be described through the following dynamic equilibrium equation:

$$\mathbf{M}\ddot{\mathbf{u}}(t) + \mathbf{C}\dot{\mathbf{u}}(t) + \mathbf{f}_{\mathrm{nl}}(t) = \mathbf{f}(t;\bar{v}_y, \alpha) \tag{3}$$

where $\dot{\mathbf{u}}(t)$ and $\ddot{\mathbf{u}}(t)$ are the velocity and acceleration response vectors, $\mathbf{M}$ and $\mathbf{C}$ are the mass and damping matrices of the system, $\mathbf{f}(t;\bar{v}_y, \alpha)$ is the external dynamic wind load with $\bar{v}_y$ the wind speed of MRI y at the building top (i.e. the intensity measure im) and α the direction of $\bar{v}_y$ with respect to the building, while $\mathbf{f}_{\mathrm{nl}}(t)$ is a vector of non-linear restoring forces. Following general plasticity theory [30–32], $\mathbf{f}_{\mathrm{nl}}(t)$ can be written as:

$$\mathbf{f}_{\mathrm{nl}}(t) = \mathbf{B}^T\mathbf{Q}(t) = \mathbf{B}^T\mathbf{E}[\boldsymbol{\epsilon}(t) - \boldsymbol{\epsilon}_p(t)] \tag{4}$$

where $\mathbf{E} = \mathrm{diag}[\mathbf{E}_1, ..., \mathbf{E}_m]$ is the block-diagonal matrix collecting the elastic stiffness matrices of the m members composing the structural system; $\mathbf{B}$ is a compatibility matrix that in small deformation theory depends exclusively on the undeformed configuration of the system; $\mathbf{Q}(t)$ is the generalized stress history response (i.e. internal force histories in the critical sections of the structure); $\boldsymbol{\epsilon}(t)$ are the corresponding generalized strain histories (i.e. relative rotations and axial deformations) that must satisfy the compatibility conditions

$$\boldsymbol{\epsilon}(t) = \mathbf{B}\mathbf{u}(t) \tag{5}$$

with $\mathbf{u}(t)$ the global displacement response of the system; while $\boldsymbol{\epsilon}_p(t)$ is the generalized plastic strain response of the system.

Under the assumption of elastic perfectly plastic (EPP) material behavior, piece-wise linearization of the yield surfaces associated with each critical section of the structural system, and associated plastic flow, $\boldsymbol{\epsilon}_p(t)$ will be governed by the following equations:

$$\boldsymbol{\varphi}(t) = \mathbf{N}^T\mathbf{Q}(t) - \mathbf{R} \leqslant \mathbf{0} \tag{6a}$$

$$\boldsymbol{\varphi}^T(t)\dot{\boldsymbol{\lambda}}(t) = \dot{\boldsymbol{\varphi}}^T(t)\dot{\boldsymbol{\lambda}}(t) = 0 \tag{6b}$$

$$\dot{\boldsymbol{\epsilon}}_p(t) = \mathbf{N}\dot{\boldsymbol{\lambda}}(t), \qquad \dot{\boldsymbol{\lambda}}(t) \geqslant \mathbf{0} \tag{6c}$$

where $\boldsymbol{\varphi}$ represents the yield functions (i.e. the interaction domains of the potential plastic hinges), $\mathbf{N}$ is the block diagonal matrix collecting the unit external normals to the piece-wise linear yield surfaces defining the yield functions, $\mathbf{R}$ is the plastic resistance vector, while $\dot{\boldsymbol{\lambda}}$ is the vector of plastic multiplier rates. In particular, Eq. (6a) represents the yield condition that requires a generalized stress point to remain in the yield domain of the cross section (i.e. within the interaction domain of a potential plastic hinge) while Eqs. (6a) and (6b) govern the loading-unloading process and confer to the system a path-dependent nature.

Finally, Eq. (6c) expresses the normality rule. At this juncture, it should be observed that, while EPP material behavior will be assumed in this work, the governing elastoplastic equations of Eqs. (6a)–(6c) can be formulated for a wide class of material constitutive laws [31], as can the dynamic shakedown problem that will be introduced in the following [e.g., 33,34]. The interest in considering an EPP material behavior stems from how it enables not only a straightforward formulation of the shakedown problem, but also the straightforward inelastic modeling of steel structures without precluding the inelastic modeling of reinforced concrete structures [e.g., 35].

Eqs. (3)–(5), (6a)–(6c) together with the following initial conditions

$$\mathbf{u}(0) = \mathbf{u}_0, \qquad \dot{\mathbf{u}}(0) = \dot{\mathbf{u}}_0 \tag{7}$$

govern the dynamic EPP response of structural systems discretized into m frame elements with potential plastic hinge yielding at their extremes. In particular, the resolution of this problem generally requires the adoption of a step-by-step integration scheme [36,31,37] of a non-trivial computational effort, especially for long duration external load histories (e.g. typical dynamic wind load histories).

4. Dynamic shakedown

4.1. Definition and classic solution

If during the dynamic EPP response the plastic deformations $\boldsymbol{\epsilon}_p(t)$ become constant, i.e. time independent, the structure is said to have adapted or reached a state of "dynamic shakedown". In other words, a finite field of plastic strains have formed allowing the structure to respond in a purely elastic regime for the remainder of the load history [24]. This state is of particular interest as it rules out the uncontrolled growth of plastic deformation over the load history, i.e. incremental plastic collapse (ratcheting), and of alternating plasticity that can lead to low cycle fatigue failure.

A criterion for the determination of the state of "dynamic shakedown" for a fully specified load history $\mathbf{f}_\infty(t)$ of infinite duration, i.e. from $t = 0$ to $t = +\infty$, can be announced as [22,38,24]: a necessary and sufficient condition for dynamic shakedown is that there exists a finite time $t^* \geqslant 0$ and some arbitrary initial conditions $(\mathbf{u}_0^*, \dot{\mathbf{u}}_0^*)$ for which the following holds:

$$\mathbf{N}^T(\mathbf{Q}^E(t) + \boldsymbol{\rho}) - \mathbf{R} \leqslant \mathbf{0}, \qquad \forall\, t \geqslant t^* \tag{8}$$

where $\mathbf{Q}^E(t)$ is the purely elastic generalized stress response to $\mathbf{f}_\infty(t)$ with initial conditions $(\mathbf{u}_0^*, \dot{\mathbf{u}}_0^*)$, while $\boldsymbol{\rho}$ is a time independent generalized self stress distribution (associated with the time independent plastic distortions enabling shakedown) that, when summed to $\mathbf{Q}^E(t)$, ensures that the generalized stress response of the system satisfies the yield condition of Eq. (6a) for $t \geqslant t^*$.

In general, the verification of the criterion announced above is not straightforward. A special case that significantly simplifies the problem, and which will be seen to be of interest to this work, is when the external load $\mathbf{f}_\infty(t)$ is not only of infinite duration but also periodic with period T (indicated in the following as $\widetilde{\mathbf{f}}_\infty(t)$). Indeed, under these circumstances, shakedown will occur if a time independent generalized stress distribution, $\boldsymbol{\rho}$, can be found for which Eq. (8) is satisfied for the steady state elastic response in $[0, T]$ [22,38,24]. Because only the steady state elastic response is now required, the problem of verifying whether shakedown occurs has become independent of the choice of initial conditions $(\mathbf{u}_0^*, \dot{\mathbf{u}}_0^*)$.

4.1.1. Dynamic shakedown multiplier: classic solution

A classic problem of interest in dynamic shakedown is the estimation of the dynamic shakedown multiplier s_p, defined as the maximum amplification that the external loads $\widetilde{\mathbf{f}}_\infty(t)$ can undergo before shakedown no longer occurs, i.e. the conditions of Eq. (8) can no longer be satisfied. It can be shown that, under the assumption of piece-wise linear yield surfaces and infinite duration periodic loads, the search for s_p can be posed in the form of the following linear programming problem (LPP):

$$\begin{aligned} &s_p = \max_{s,\boldsymbol{\rho}} s \\ &\text{subject to} \\ &\bar{\mathbf{Q}}^s = \max_{0 \leqslant t \leqslant T} [\mathbf{N}^T \mathbf{Q}_s^E(t)] \\ &\boldsymbol{\varphi}_s = s\bar{\mathbf{Q}}^s + \mathbf{N}^T\boldsymbol{\rho} - \mathbf{R} \leqslant \mathbf{0} \\ &\mathbf{B}^T\boldsymbol{\rho} = \mathbf{0} \end{aligned} \tag{9}$$

where $\boldsymbol{\varphi}_s$ is the amplified and time maximized yield function with $\boldsymbol{Q}_s^E(t)$ the purely elastic steady state generalized stress response in $[0, T]$, while $\bar{\boldsymbol{Q}}^s$ is the maximum generalized stress demand for each linearized yield mode of each critical section of the system. The last condition in Eq. (9) ensures that the generalized stress state associated with the plastic distortions occurring during shakedown are self-equilibrated. It should be observed that by setting $\boldsymbol{\rho} = \mathbf{0}$, the LLP of Eq. (9) will provide an estimate of the elastic multiplier s_e, i.e. the maximum amount the external loads $\widetilde{\mathbf{f}}_\infty(t)$ can be amplified before inelasticity will occur [19].

4.2. A strain-driven formulation of dynamic shakedown

The resolution of the LPP of Eq. (9) provides a classic solution to the dynamic shakedown problem in terms of s_p. A limitation of this approach is that it does not provide any information on the entity of the time independent plastic strains, $\boldsymbol{\epsilon}_p$, occurring during the adaption process. Therefore, if the inelastic deformations are required, an alternative approach to estimate shakedown has to be explored. To this end, the algorithms proposed in [39,35] for estimating the shakedown multiplier in quasi-static conditions are of interest. Indeed, these algorithms are based on using a path-following scheme which provides, as a byproduct, estimates of the plastic strains and deformations associated with reaching the state of shakedown. Unfortunately, these estimates are associated with a simulated load path and not the actual load path followed by the structure in reaching shakedown. However, by first extending these algorithms to dynamic shakedown problems, it can be observed that, under the conditions outlined in Section 4.2.3, direct estimations of the plastic strains and deformations occurring during shakedown can be made.

4.2.1. Problem formulation

To formulate the dynamic shakedown problem for periodic and infinite duration dynamic loads in terms of strains and displacements, it is convenient to first consider a residual displacement increment $\mathbf{u}_r$ together with a load multiplier s satisfying $s_e \leqslant s \leqslant s_p$. From $\mathbf{u}_r$ the following strain increment can be defined [39]:

$$\boldsymbol{\epsilon}_r = \mathbf{B}\mathbf{u}_r \tag{10}$$

An admissible stress vector, $\boldsymbol{\rho}$, corresponding to $\mathbf{u}_r$ and s can be obtained through the following return mapping scheme:

$$\boldsymbol{\rho}(s, \mathbf{u}_r) = \boldsymbol{\rho}_E + \Delta\boldsymbol{\rho}, \qquad \boldsymbol{\varphi}_s(s, \boldsymbol{\rho}) \leqslant 0 \tag{11}$$

where $\boldsymbol{\rho}_E = \boldsymbol{\rho}_0 + \mathbf{E}\mathbf{B}\mathbf{u}_r$ is the elastic predictor of $\boldsymbol{\rho}$ with $\boldsymbol{\rho}_0$ an initial generalized stress distribution, while $\Delta\boldsymbol{\rho} = -\mathbf{E}\,\boldsymbol{\epsilon}_p$ with $\boldsymbol{\epsilon}_p$ the plastic part of the strain increment $\boldsymbol{\epsilon}_r$ which is defined by the Kuhn-Tucker condition:

$$\boldsymbol{\epsilon}_p = \mathbf{N}\boldsymbol{\lambda}, \qquad \lambda_i = \begin{cases} = 0 & \text{if} \quad \varphi_{si}(s, \boldsymbol{\rho}_E) < 0 \\ \geqslant 0 & \text{if} \quad \varphi_{si}(s, \boldsymbol{\rho}_E) \geqslant 0 \end{cases} \quad \text{for} \quad i = 1, \ldots, N_s \tag{12}$$

with λ_i the ith component of the plastic multiplier vector $\boldsymbol{\lambda}$ and N_s the total number of yield modes of the system. Instead of estimating $\boldsymbol{\rho}(s, \mathbf{u}_r)$ by directly solving the return mapping of Eqs. (11) and (12), $\boldsymbol{\rho}(s, \mathbf{u}_r)$ can be more conveniently estimated by minimizing the Haar-Kàrmàn function subject to the dynamic shakedown feasibility conditions:

$$\min_{\Delta\boldsymbol{\rho}} \tfrac{1}{2}\Delta\boldsymbol{\rho}^T\mathbf{E}^{-1}\Delta\boldsymbol{\rho}$$
subject to
$$\bar{\mathbf{Q}}^s = \max_{0\leqslant t\leqslant T}[\mathbf{N}^T\mathbf{Q}_s^E(t)]$$
$$\varphi_s = s\bar{\mathbf{Q}}^s + \mathbf{N}^T(\boldsymbol{\rho}_E + \Delta\boldsymbol{\rho}) - \mathbf{R} \leqslant \mathbf{0} \tag{13}$$

Eq. (13) represents a standard strictly convex quadratic programming problem that can be efficiently solved in high dimensions through standard optimization algorithms. By solving the return mapping scheme for given values of s and $\mathbf{u}_r$, solutions in terms of $\boldsymbol{\rho}(s, \mathbf{u}_r)$ will be found that satisfy the shakedown feasibility condition $\varphi_s(s, \boldsymbol{\rho}) \leqslant 0$. However, for $\boldsymbol{\rho}(s, \mathbf{u}_r)$ to satisfy the dynamic shakedown criterion of Section 4.1, it must also be self-equilibrated. This requirement can be imposed in terms of the internal force vector, $\mathbf{S}$, associated with the residual displacement increment $\mathbf{u}_r$ and multiplier s as:

$$\mathbf{S}(s, \mathbf{u}_r) = \mathbf{B}^T\boldsymbol{\rho}(s, \mathbf{u}_r) = \mathbf{0} \tag{14}$$

By combining this condition with the strain-driven scheme for the identification of admissible values of $\boldsymbol{\rho}(s, \mathbf{u}_r)$, the following dynamic shakedown problem can be stated directly in terms of the residual displacement increments:

$$s_p = \max s\colon \exists\ \mathbf{u}_r\colon \mathbf{S}(s, \mathbf{u}_r) = \mathbf{0} \tag{15}$$

To solve Eq. (15), an incremental iterative scheme can be adopted based on producing a sequence of admissible safe states that are self-equilibrated.

4.2.2. An iterative solution scheme

Commencing from the elastic limit state ($s = s_e$, $\boldsymbol{\rho} = \mathbf{0}$, $\mathbf{u}_r = \mathbf{0}$), the iterative solution method estimates the shakedown multiplier s_p and the corresponding admissible self-equilibrated stress state $\boldsymbol{\rho}$ with associated residual displacement vector $\mathbf{u}_r$ by producing a sequence of admissible safe states ($s^{(k)}$, $\boldsymbol{\rho}^{(k)}$, $\mathbf{u}_r^{(k)}$) with $s^{(k)}$ monotonously increasing at each step and convergent to s_p. The overall procedure is outlined in the flowchart of Fig. 1. In particular, at each step, the multiplier s and residual displacement field $\mathbf{u}_r$ are initialized through the following equations:

$$s_1 = s^{(k-1)} + \beta(s^{(k-1)} - s^{(k-2)})$$
$$\mathbf{u}_{r1} = \mathbf{u}_r^{(k-1)} + \beta(\mathbf{u}_r^{(k-1)} - \mathbf{u}_r^{(k-2)}) \tag{16}$$

with β an appropriate scaling factor. The iterative process within each step k produces a monotonically decreasing sequence, indexed with j, of nodal forces $\mathbf{S}(s, \mathbf{u}_r)$ until the self-equilibrated condition $\mathbf{S}(s_j, \mathbf{u}_{rj}) = \mathbf{0}$ is satisfied. To obtain this sequence, s_j and $\mathbf{u}_{rj}$ are updated at the jth iteration through the condition:

$$\begin{cases}\mathbf{S}(s_j, \mathbf{u}_{rj}) + \mathbf{K}_j\dot{\mathbf{u}}_{rj} + \mathbf{y}_j\dot{s}_j = \mathbf{0}\\ \mathbf{y}_j^T\dot{\mathbf{u}}_{rj} = 0\end{cases} \tag{17}$$

where $\mathbf{S}(s_j, \mathbf{u}_{rj})$ is estimated by solving for $\boldsymbol{\rho}_j(s_j, \mathbf{u}_{rj})$ through Eqs. (11) and (13), $\mathbf{K}_j$ and $\mathbf{y}_j$ are the initial tangent in $(s_j, \mathbf{u}_{rj})$ of the nodal force $\mathbf{S}(s_j, \mathbf{u}_{rj})$ given by

$$\begin{cases}\mathbf{K}_j = \dfrac{\partial\mathbf{S}(s, \mathbf{u}_r)}{\partial\mathbf{u}_r}\Big|_{(s_j, \mathbf{u}_{rj})}\\ \mathbf{y}_j = \dfrac{\partial\mathbf{S}(s, \mathbf{u}_r)}{\partial s}\Big|_{(s_j, \mathbf{u}_{rj})}\end{cases} \tag{18}$$

while $\dot{\mathbf{u}}_{rj}$ and $\dot{s}$ are corrections estimated as follows, together with the updated values of the multiplier and residual displacement field:

$$\begin{cases}\dot{\mathbf{u}}_{rj} = -\mathbf{K}_j^{-1}(\mathbf{S}_j + \dot{s}_j\mathbf{y}_j)\\ \dot{s}_j = -\dfrac{\mathbf{y}_j^T\mathbf{K}_j^{-1}\mathbf{S}_j}{\mathbf{y}_j^T\mathbf{K}_j^{-1}\mathbf{y}_j}\end{cases} \quad \text{and} \quad \begin{cases}\mathbf{u}_{rj+1} = \mathbf{u}_{rj} + \dot{\mathbf{u}}_{rj}\\ s_{j+1} = s_j + \dot{s}_j\end{cases} \tag{19}$$

To improve the efficiency of the solution process and to guarantee convergence of the iterative scheme, $\mathbf{K}_j$ can be taken as the elastic stiffness matrix of the system $\mathbf{K}$, defined at the start of the process [35].

The solution provided at each step k satisfies the plastic admissibility and self-equilibrium condition while the multiplier $s^{(k)}$ is less than or equal to s_p. As such, the solution process is terminated when $s^{(k)} = s^{(k-1)}$, providing the shakedown multiplier.

In addition to the total self-stresses, $\boldsymbol{\rho}$, and residual displacements, $\mathbf{u}_r$, the solution process can also produce estimates of the total plastic strains to occur during the shakedown process, $\boldsymbol{\epsilon}_p$, through the following expression:

$$\boldsymbol{\epsilon}_p = \sum_{k=0}^{K}\boldsymbol{\epsilon}_p^{(k)} = \sum_{k=0}^{K}\left(\mathbf{B}\mathbf{u}_r^{(k)} - \mathbf{E}^{-1}\boldsymbol{\rho}^{(k)}\right) \tag{20}$$

with K the total number of steps required in obtaining s_p.

Before closing this section, it should be observed that significant computational gains over direct integration are expected from the implementation of the proposed algorithm. Indeed, for a given load history of duration T, the algorithm outlined above only requires the estimation of elastic dynamic response in $[0, T]$ for unamplified loads. Moreover, the iterative process of Fig. 1 only has to be carried out once, at the peak steady state elastic responses $\bar{\mathbf{Q}}^s$, for a given load history of arbitrary length T. In other words, a single non-linear problem is solved in $[0, T]$ as opposed to the multiple non-linear problems that are solved in $[0, T]$ when implementing direct integration methods. By observing that at each internal iteration j the iterative process of Fig. 1 only requires the resolution of a strictly convex QPP (i.e. a problem type that can be efficiently solved through well established optimization algorithms), significant computational gains over direct integration are expected. In particular, the longer the load duration, the greater the expected computational gains. The only potential challenge of the proposed approach lies in the number of internal, j, and external, k, iterations necessary before convergence. However, by adopting $\mathbf{K}$ in place of $\mathbf{K}_j$, convergence of the scheme is guaranteed [39].

4.2.3. The simulated load path

The load path of the strain-based scheme of Section 4.2.2 is defined in terms of the peak steady state purely elastic dynamic response to $\tilde{\mathbf{f}}_\infty(t)$, i.e. in terms of the generalized stress $\bar{\boldsymbol{Q}}^s$ that appears in Eq. (13). The actual load path depends on the elastoplastic dynamic response to $\tilde{\mathbf{f}}_\infty(t)$. The two paths will differ due to: (1) elastoplastic vs. elastic material behavior; and (2) the initial conditions ($\mathbf{u}_0$, $\dot{\mathbf{u}}_0$) that generally cause transient dynamic effects. The steady state response assumption of the simulated load path implies that plastic strain and deformations caused by any transient dynamic effects cannot be captured by the strain-based scheme. However, if it is assumed that each period of the load $\tilde{\mathbf{f}}_\infty(t)$ starts with the structure at rest, then the purely elastic response of the structure estimated for the homogeneous initial conditions:

$$\mathbf{u}(0) = \mathbf{0}, \quad \dot{\mathbf{u}}(0) = \mathbf{0} \tag{21}$$

will coincide with the steady state elastic response to $\tilde{\mathbf{f}}_\infty(t)$. Under these conditions, the only difference between the simulated and actual load paths is in how, for the actual load path, plastic strains and deformations are produced in the peaks of the path dependent elastoplastic generalized stress $\boldsymbol{Q}_s^{EP}(t)$ as opposed to the peaks of the path dependent elastic generalized stress $\boldsymbol{Q}_s^E(t)$. Because for moderate inelasticity, i.e. shakedown occurs, these peaks must be closely related, the simulated load path should provide a good approximation of the plastic strain and deformations occurring in reaching shakedown under the prescribed load $\tilde{\mathbf{f}}_\infty(t)$.

Before closing this section, it should be observed that the requirement that the structure be at rest at the start of the load period T is not restrictive for the systems of interest to this work. Indeed, there will always be a period of calm before a major windstorm during which time the structure will come to a rest due to damping. It should be observed that, from the estimation of the plastic strains and deformations, peak responses at shakedown can be directly estimated as:

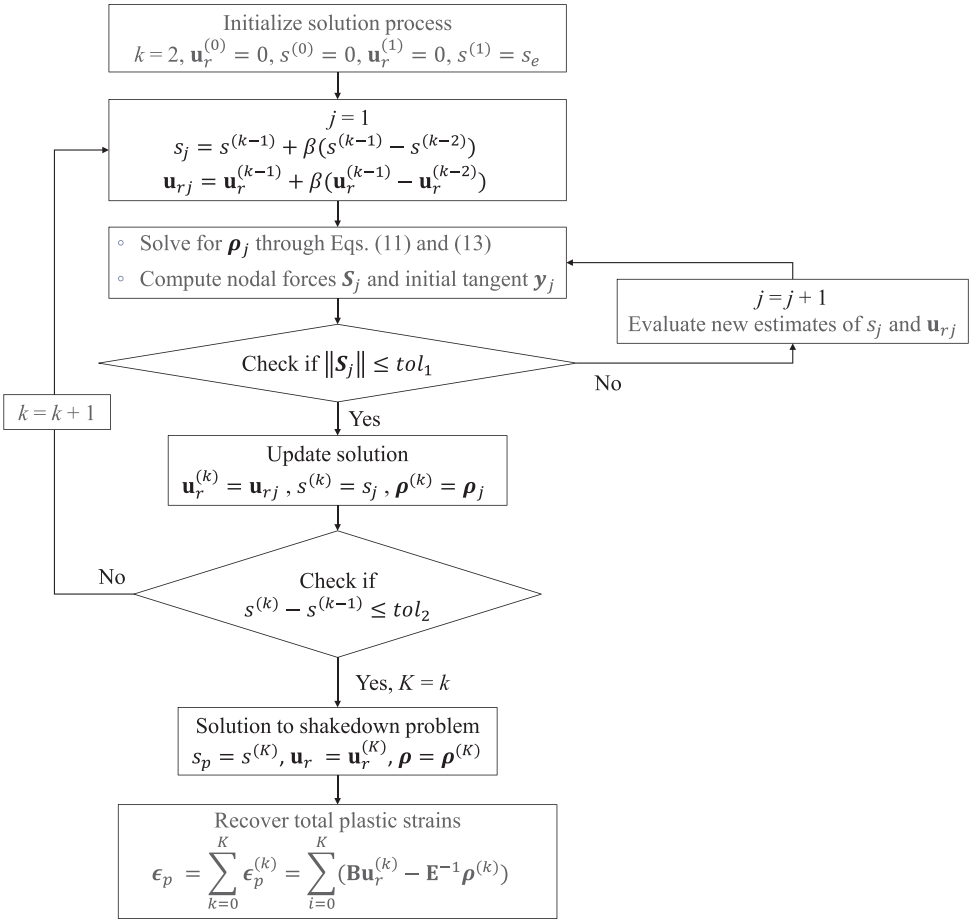

Fig. 1. Flowchart of the strain-based dynamic shakedown algorithm.

$$\hat{\mathbf{u}} = \mathbf{u}_r + \max_{0 \le t \le T} [\mathbf{u}_s^E(t)], \quad \hat{\epsilon} = \epsilon_p + \max_{0 \le t \le T} [\epsilon_s^E(t)] \tag{22}$$

where $\mathbf{u}_s^E(t)$ and $\epsilon_s^E(t)$ are the purely elastic displacement and strain response at shakedown. Finally, it can be observed that the strain-based iterative scheme is capable of estimating plastic strains and deformations for any multiplier value, s, satisfying $s \in [s_e, s_p]$. Indeed, under these circumstances, it is simply necessary to terminate the strain-based iterative scheme once s is reached.

5. A probabilistic collapse estimation framework

As discussed in Section 2, the ultimate goal of this work is to define a probabilistic framework based on dynamic shakedown for the estimation of $P(C|im)$ and therefore of the probability of collapse of a structure subject to a windstorm of direction α and intensity $im = \bar{v}_y$. To this end, the following collapse modes are considered:

1. The inability of the structure to reach the state of dynamic shakedown. This leaves the structure at risk of collapse due to ratcheting (progressive collapse), low cycle fatigue (failure due to alternating plasticity) and instantaneous plastic collapse.
2. Excessive peak $\hat{\mathbf{u}}$ and/or residual $\mathbf{u}_r$ displacements/drifts at shakedown. Excessive peak displacements/drifts leave the structure susceptible to global instability, while excessive residual deformations can lead to structures that are unstable/irreparable after the event (it should be observed that, if necessary, P-Delta effects can be included in the proposed framework through methods similar to those outlined in [40]).
3. Excessive plastic deformations ϵ_p and/or local member response at shakedown. Excessive local beam and column response can lead to member failure.

In defining the first collapse mode, the inability to reach dynamic shakedown is here interpreted as the shakedown multiplier s_p, estimated through solving the LPP problem of Eq. (9), assuming a value less than 1. It should be observed that, while failure to find solutions to the LPP of Eq. (9) is highly unlikely due to the convexity of LPPs (i.e. no local minima) and the wide availability of robust optimization algorithms with proven convergence properties for their resolution (i.e. simplex algorithm/interior point methods), the estimation of the first collapse mode is based on the results of a numerical algorithm solved to within a convergence tolerance.

Given an appropriate periodic and infinite duration stochastic wind load model, the conditions outlined above can be probabilistically characterized through combing Monte Carlo simulation with the strain-based dynamic shakedown framework of Section 4.2. The first step towards this goal is therefore the definition of an appropriate stochastic wind loads model.

5.1. Wind load model

A straightforward approach for defining an infinite duration and periodic load from any given wind load history $\mathbf{f}(t;\bar{v}_y, \alpha)$ of interest is to simply consider $\mathbf{f}(t;\bar{v}_y, \alpha)$ infinitely repeated. This "artificial" windstorm can be formally defined as:

$$\tilde{\mathbf{f}}_\infty\Big(t + nT;\bar{v}_y, \alpha\Big) = \mathbf{f}\Big(t;\bar{v}_y, \alpha\Big) \quad \text{for} \begin{cases} n = 0, 1, \ldots, +\infty \\ t \in [0, T] \end{cases} \tag{23}$$

and is illustrated in Fig. 2. In defining $\tilde{\mathbf{f}}_\infty(t;\bar{v}_y, \alpha)$, it is important to observe that the application of the proposed approach for determining

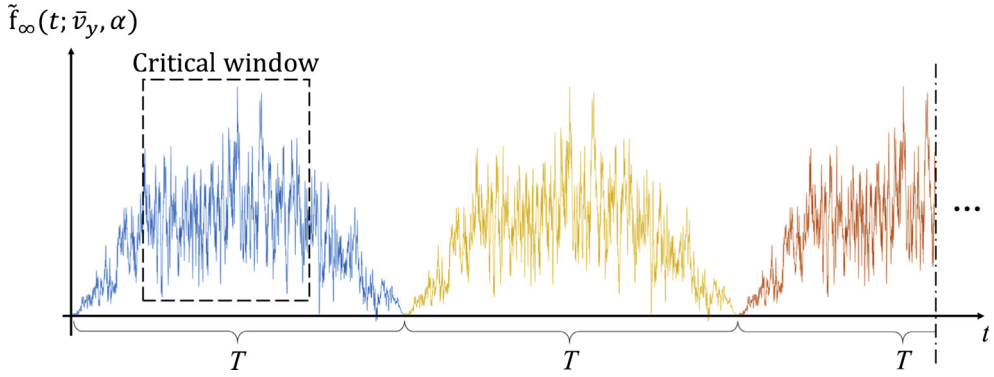

Fig. 2. Illustration of a generic component of $\tilde{\mathbf{f}}_\infty$ for a windstorm of duration T.

whether a structural system subject to $\tilde{\mathbf{f}}_\infty(t;\bar{v}_y,\alpha)$ will shakedown, and if so the entity of the plastic deformations and strains at shakedown, only requires the estimation of the purely elastic steady state dynamic response over one period of $\tilde{\mathbf{f}}_\infty(t;\bar{v}_y,\alpha)$. In particular, if it is assumed that inelastic behavior will only occur over a critical window of the period (e.g. in the maximum stationary segment of the windstorm as illustrated in Fig. 2), then the elastic steady state response estimation is only required in the critical window. To fully appreciate the computational savings of the proposed approach, it should be recalled that to estimate the plastic deformations and strains at shakedown through direct integration, full dynamic elastoplastic solutions over a number of cycles of $\tilde{\mathbf{f}}_\infty(t;\bar{v}_y,\alpha)$ would be necessary. Finally, it should be observed that the elastic stress response is in a "steady state" under a periodic load when the free-vibration response associated with an arbitrary set of initial conditions damps out. In particular, as discussed in Section 4.2.3, to ensure that the system is always in a steady state, it is simply necessary to assume that the structure is at rest at the beginning of each load repetition (i.e. there is a period of calm between each load repetition that allows the structure to come to a rest due to damping). This condition is independent of how the loads vary in each period of loading, i.e. the form of the load history in $[0, T]$ does not affect how, under the aforementioned conditions, the structure's elastic response will always be steady state. Therefore, $\mathbf{f}(t;\bar{v}_y,\alpha)$ can be a realization of a stationary or non-stationary stochastic process. This enables the consideration of both synoptic and non-synoptic wind events in the proposed framework.

5.1.1. Stochastic representation of the wind load history

In order to study the record to record variability in the inelastic response of the system, multiple wind load histories are required, i.e. multiple realizations of $\tilde{\mathbf{f}}_\infty(t;\bar{v}_y,\alpha)$, and therefore of $\mathbf{f}(t;\bar{v}_y,\alpha)$, are necessary. From a probabilistic standpoint, $\mathbf{f}(t;\bar{v}_y,\alpha)$ can be viewed as a vector-valued stochastic process [41]. In particular, an efficient approach for the simulation of $\mathbf{f}$ is to decompose the N-dimensional vector $\mathbf{f}$ into N independent vector valued subprocesses through spectral proper orthogonal decomposition (POD) and therefore as [42–44,41,45]:

$$\mathbf{f}\left(t;\bar{v}_y,\alpha\right)=\sum_{j=1}^{N}\mathbf{f}_j\left(t;\bar{v}_y,\alpha\right) \tag{24}$$

where $\mathbf{f}_j(t)$ is the jth subprocess which can be given the following spectral representation:

$$\mathbf{f}_j(t;\bar{v}_y,\alpha)=\sum_{k=1}^{K}\left|\boldsymbol{\Psi}_j(\omega_k;\alpha)\right|\sqrt{2\Lambda_j(\omega_k;\bar{v}_y,\alpha)\Delta\omega}\times\cos\left(\omega_k t+\theta_j(\omega_k)+\vartheta_{kj}\right) \tag{25}$$

where Λ_j and $\boldsymbol{\Psi}_j$ are the jth frequency dependent eigenvalue and eigenvector of $\mathbf{f}$, K is the total number of discrete frequencies considered in the interval $[0, K\Delta\omega]$ with $\Delta\omega$ the frequency increment that is related to the Nyquist (cutoff) frequency through $\omega_{\text{Nyquist}}=K\Delta\omega/2$, $\omega_k=k\Delta\omega$, $\boldsymbol{\theta_j}$ is a vector of complex angles, while ϑ_{kj} are independent and uniformly distributed random variables in $[0, 2\pi]$. In particular, the ith component of $\boldsymbol{\theta_j}$ can be estimated as:

$$\theta_{ji}(\omega_k)=\tan^{-1}\left\{\frac{\text{Im}[\Psi_{ji}(\omega_k)]}{\text{Re}[\Psi_{ji}(\omega_k)]}\right\} \tag{26}$$

with $\text{Im}[\Psi_{ij}(\omega_k)]$ and $\text{Re}[\Psi_{ij}(\omega_k)]$ the imaginary and real parts of the ith component of $\boldsymbol{\Psi}_j$.

To ensure a complete description of the complex aerodynamic response of typical high-rise structures (e.g. acrosswind wake-induced vortex shedding), in this work the frequency dependent eigenvalues and eigenvectors of $\mathbf{f}$ are estimated directly from wind tunnel data. This will ensure that any aerodynamic phenomena captured in the wind tunnel tests will be present in the simulated load histories. To generate realizations of $\mathbf{f}(t;\bar{v}_y,\alpha)$ following the model outlined above, the subprocesses are first generated through the Fast Fourier Transform approach [46] and then combined as indicated in Eq. (24). The possibility to generate the subprocesses independently while considering only the first few spectral POD modes of $\mathbf{f}$ ensures the efficiency of the approach.

5.2. Monte Carlo algorithm

From the definition of $\tilde{\mathbf{f}}_\infty(t;\bar{v}_y,\alpha)$, $P(C|\bar{v}_y)$ can be estimated for a given wind direction α, and in terms of the collapse conditions outlined at the beginning of Section 5 as:

$$P\left(C\middle|\bar{v}_y\right)=\frac{1}{N_s}\sum_{i=1}^{N_s}I_C^{(i)}\left(\bar{v}_y,\alpha\right) \tag{27}$$

where N_s is the total number of samples used in the simulation while $I_C^{(i)}$ is the following indicator function evaluated for $(\bar{v}_y,\alpha)$ as:

$$I_C^{(i)}=\begin{cases}1 & \text{if } (s_p^{(i)}<1)\cup(\mathbf{u}_r^{(i)}>\tilde{\mathbf{u}}_r)\cup(\hat{\mathbf{u}}^{(i)}>\tilde{\hat{\mathbf{u}}})\cup(\boldsymbol{\epsilon}_p^{(i)}>\tilde{\boldsymbol{\epsilon}}_p)\\ 0 & \text{if otherwise}\end{cases} \tag{28}$$

where $s_p^{(i)}$, $\mathbf{u}_r^{(i)}$, $\hat{\mathbf{u}}^{(i)}$, and $\boldsymbol{\epsilon}_p^{(i)}$ are the ith sample of the shakedown multiplier, residual displacements, peak displacements, and plastic strains at shakedown, while $\tilde{\mathbf{u}}_r$, $\tilde{\hat{\mathbf{u}}}$, and $\tilde{\boldsymbol{\epsilon}}_p$ are user defined collapse limits set respectively on $\mathbf{u}_r$, $\hat{\mathbf{u}}$, and $\boldsymbol{\epsilon}_p$. A flowchart of the overall procedure for evaluating Eq. (27) through the indicator function of Eq. (28) is shown in Fig. 3. In particular, the step-by-step Monte Carlo algorithm is as follows:

1. Set the intensity $\bar{v}_y$ and direction α of the windstorm of interest. Set $i=0$.
2. Generate a realization of $\tilde{\mathbf{f}}_\infty(t;\bar{v}_y,\alpha)$ through the stochastic wind load model of Section 5.1.1 after calibration to appropriate wind tunnel data. Set $i=i+1$.

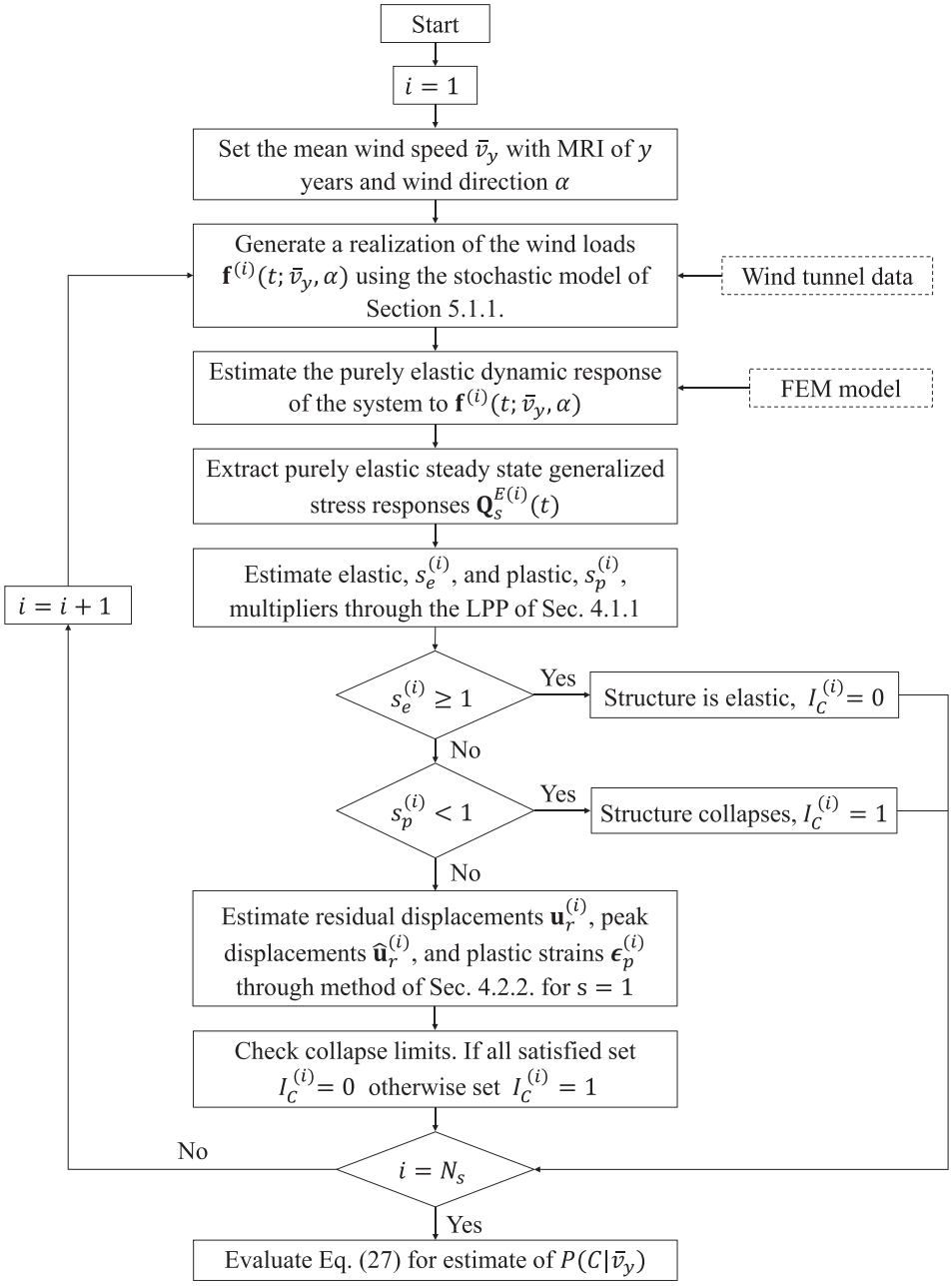

Fig. 3. Flowchart of the overall simulation strategy.

3. Calculate the steady state elastic generalized stress response $\mathbf{Q}_s^E(t)$ in $[0, T]$ for the load history of step 2 using any dynamic elastic analysis procedure (e.g. direct integration of the elastic modal equations).
4. Estimate the elastic and plastic multipliers, s_e and s_p, by solving the linear programming problem of Eq. (9) with $\boldsymbol{\rho} = \mathbf{0}$.
5. If $s_e \geqslant 1$ (i.e. the structure remains elastic) set $\mathbf{u}_r^{(i)} = \mathbf{0}$, $\boldsymbol{\epsilon}_p^{(i)} = \mathbf{0}$, and $I_C^{(i)} = 0$ and return to step 2.
6. If $s_p < 1$ (i.e. structure collapses for $s = 1$ due to lack of shakedown) set $I_C^{(i)} = 1$ and return to step 2.
7. If $s_e < 1$ and $s_p \geqslant 1$, then estimate the residual displacements, $\mathbf{u}_r$, peak displacements $\hat{\mathbf{u}}_r$, and strains, $\boldsymbol{\epsilon}_p$, for the unamplified windstorm, i.e. $s = 1$, using the strain-based scheme of Section 4.2.
8. Check if any of the collapse limits ($\tilde{\mathbf{u}}_r$, $\tilde{\hat{\mathbf{u}}}$, and $\tilde{\boldsymbol{\epsilon}}_p$) have been exceeded. If yes, set $I_C^{(i)} = 1$ and return to step 2, otherwise set $I_C^{(i)} = 0$ and return to step 2.

By repeating steps 2 to 8 for N_s samples of the wind loads, the safety of the system can be estimated probabilistically using Eq. (27). In addition to the collapse probability of Eq. (27), the proposed framework can be used to directly estimate the probability distributions of the plastic strains, deformations, and peak responses at shakedown.

6. Case study

6.1. Overview

In this section, the probabilistic framework of Section 5 is illustrated on the steel frame of Fig. 4. In particular, a study on the accuracy of the simulated load path of the strain-based dynamic shakedown formulation of Section 4.2 is also presented through direct comparison to results obtained from step-by-step integration of the elastoplastic equations of Section 3.

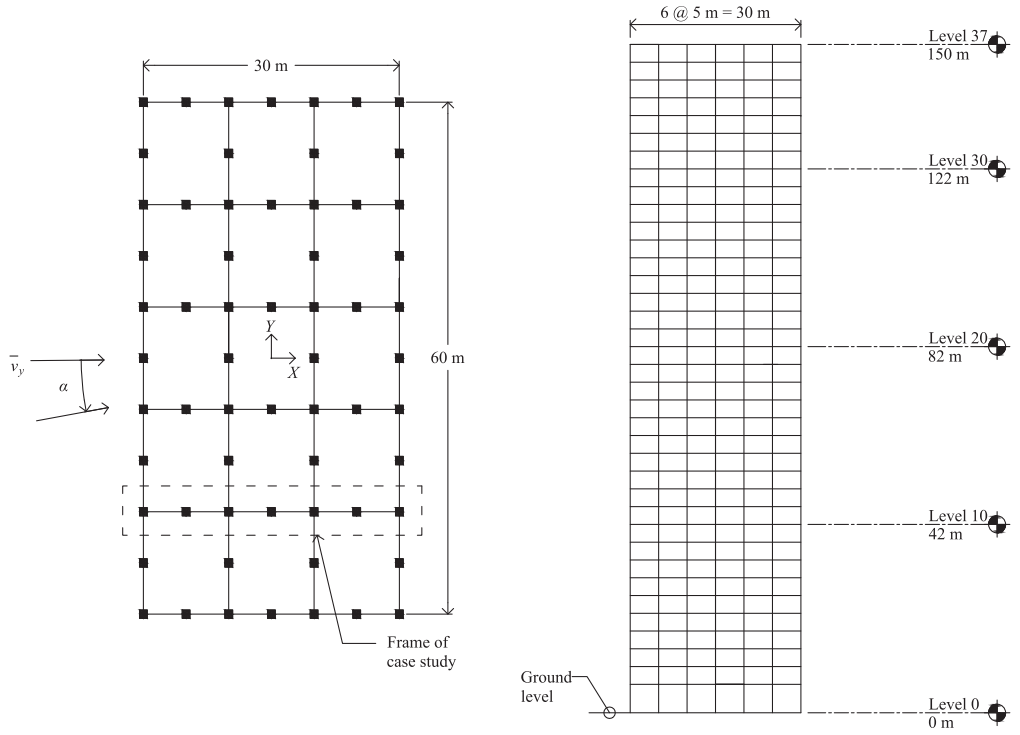

Fig. 4. Schematic of the 37-story steel frame of the case study.

6.1.1. Model description

The structure considered in this section is the 37-story six-span plane steel frame of Fig. 4 that was assumed located in the Miami region of Florida, USA. The geometry consists of beam span lengths of 5 m and interstory heights of 6 m at ground level and 4 m for all other floors. The overall height of the structure is 150 m. The columns have square box cross-sections, while the beams are wide flange standard W24 sections. The dimensions of the box columns are defined by their centerline diameters D. The thickness of the section's walls is set to $D/20$. The steel composing the frame is assumed to be elastic-perfectly plastic, and is therefore completely described by the Young's modulus E_s and yield stress σ_y, which were respectively taken as 200 GPa and 355 MPa. In particular, this last was derived from fitting a lognormal distribution to the yield strength data for Grade 50 steel reported in Appendix B of [47] and taking the threshold corresponding to the 5% percentile. The mass of the structure was lumped at each floor and calculated as the sum of the element mass and carried mass which was taken as 100 kg/m^3 and led to a super dead load of 23.5 kN/m acting on each beam element. The member sizes of the structure were determined to ensure a predominantly elastic response under the combination of dead and super dead loads mentioned above, as well as wind loads calibrated to a wind speed at the building top of $\bar{v}_y = 52.5$ m/s, which approximately corresponded to an MRI of $y = 700$ years for Miami. To estimate the wind loads given $\bar{v}_y$, the wind tunnel data described in Section 6.1.2 was used. To ensure serviceability, a 1/400 limit on the peak interstory drift ratios was imposed under wind loads calibrated to a 50 year MRI wind speed of $\bar{v}_y = 34.2$ m/s. Stability requirements for the columns were ensured by considering compact sections, as defined in [48], that had unbraced lengths that were always smaller than the limiting laterally unbraced length for full plastic bending capacity, as defined in [48]. Seismic loads were not considered as the building was assumed in the Miami region of Florida. A summary of the resulting section sizes is reported in Table 1. As designed, the first two natural frequencies of the frame were respectively $f_1 = 0.1873$ Hz and $f_2 = 0.5340$ Hz.

To evaluate the inelastic response of the structure, rigid-perfectly plastic moment hinges were assumed at the extremes of all elements for a total of 962 possible hinges. The yield domains associated with plastic hinges were defined by the ultimate moments of the sections, i.e. $M_u = \sigma_y Z$ with Z the plastic modulus of the cross section.

Table 1
Section sizes of the steel frame.

Level	Wide-flange Beams		Box Columns	
	Section size	Plastic modulus (m^3)	Section size (m)	Plastic modulus (m^3)
1–10	W24 × 192	0.0092	$D = 0.5$	0.0094
11–20	W24 × 192	0.0092	$D = 0.5$	0.0094
21–30	W24 × 103	0.0046	$D = 0.4$	0.0048
31–37	W24 × 103	0.0046	$D = 0.35$	0.0032

6.1.2. Wind loads

To simulate wind load histories, the stochastic wind load model of Section 5.1.1 was calibrated to wind tunnel data collected on a 1/300 rigid model of the building. In particular, the data was part of the Tokyo Polytechnic University's (TPU) aerodynamic database [49] and was measured considering a sampling frequency of 1000 Hz and wind speed at the building top of 11 m/s. A total of 512 pressure taps were used for 32 s of recorded data. This data was integrated and scaled therefore defining X, Y and torsional loads at the center of mass of each floor. For the application here considered, 1/6 of the X direction loads were considered acting on the moment resisting frame. These loads were used to estimate the eigenvalues Λ_j and eigenvectors $\boldsymbol{\Psi}_j$ of Eq. (25). In calibrating Eq. (25), a sampling frequency of 2 Hz was considered for a cutoff frequency of 1 Hz. When carrying out direct integration of the elastoplastic equations of Section 3, the sampling frequency was increased through linear interpolation to 100 Hz in order to ensure the stability and accuracy of the integration scheme.

6.2. Verification of the simulated load path

To illustrate the validity of the simulated load path, this section focuses on the comparison between the non-linear responses at

shakedown obtained for the 37 story frame through direct integration and those obtained from the proposed strain-based dynamic shakedown scheme. In particular, the finite element environment OpenSees (Open System for Earthquake Engineering Simulation) was used for carrying out the direct integration using a Newmark-Beta integration scheme. For the direct integration approach, Rayleigh damping was considered with damping ratios at the first two modal frequencies equal to 2.5%, while, for estimating the steady state elastic generalized stress response in the strain-based dynamic shakedown scheme, a modal integration was used while considering the first five modes with damping ratios of 2.5%. To model the rigid-perfectly plastic moment hinges in OpenSees, TwoNodeLink elements of 1 cm length were placed at the two ends of each beam and column. The moment capacity of the hinges were taken as $M_u = \sigma_y Z$ while the rotational stiffnesses were calculated based on the stiffness that would be provided by a 1 cm segment of the original elastic beam/column element.

Due to the significant computational effort involved in performing direct integration, the total length of the windstorm was set to $T = 360$ s. The first and last minute of the loads were linearly ramped to ensure approximately zero initial conditions at the beginning of each load cycle of the direct integration approach. To capture the dynamic shakedown phenomena, a total of 15 cycles were considered in the direct integration approach before returning to zero for a full cycle, as illustrated in Fig. 5 for two representative top floor time histories. This final unloading cycle allowed for the dynamic responses to completely damp out therefore enabling the direct estimation of the residual displacements and plastic rotations in the hinges. The mean wind speed at the building top was set to $\bar{v}_y = 52.5$ m/s, which approximately corresponds to an MRI of $y = 700$ years for the Miami region of Florida. To make the comparison, 200 randomly selected wind load histories were considered. Wind directions were selected from the set $\alpha \in \{0°, 10°, 20°, ..., 90°\}$ following a uniform distribution. Therefore, both alongwind and acrosswind directions were considered as well as intermediate wind directions.

6.2.1. Comparison

Fig. 6 reports the residual displacement comparison for four randomly selected alongwind ($\alpha = 0°$) and acrosswind ($\alpha = 90°$) responses. As can be seen, the residual displacements estimated through the proposed framework are almost identical to those obtained from direct integration for both incident wind directions. Plastic strains, i.e. plastic hinge rotations θ_p, corresponding to the samples generating the residual displacements fields of Fig. 6(a) and (b) are shown in Figs. 7 and 8 with hinge locations shown in Fig. 9. Once again, strong correspondence between the responses is seen. It should also be observed that, for all 200 samples, the prediction of the state of shakedown by the strain-based dynamic shakedown scheme was confirmed by the direct integration. To illustrate this, the moment rotation histories of three representative plastic hinges are shown in Figs. 10 and 11 for the

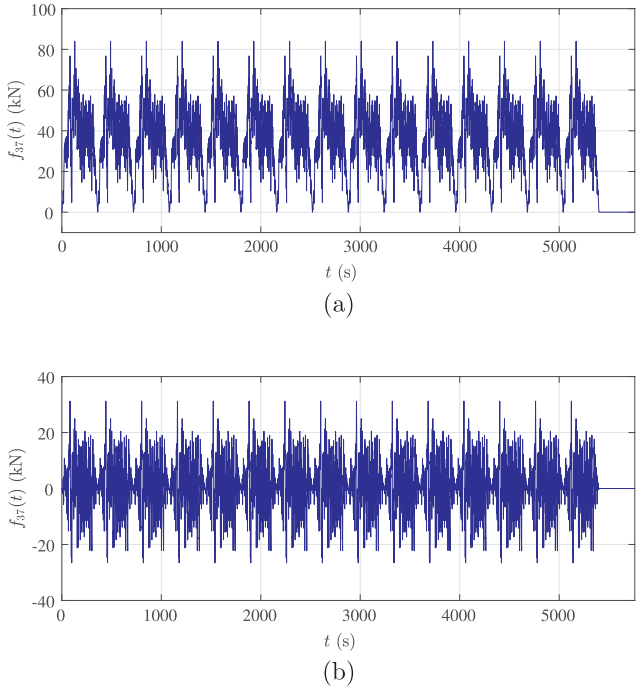

Fig. 5. A realization of the top floor stochastic wind loads for: (a) alongwind direction, i.e. $\alpha = 0°$; (b) acrosswind direction, i.e. $\alpha = 90°$.

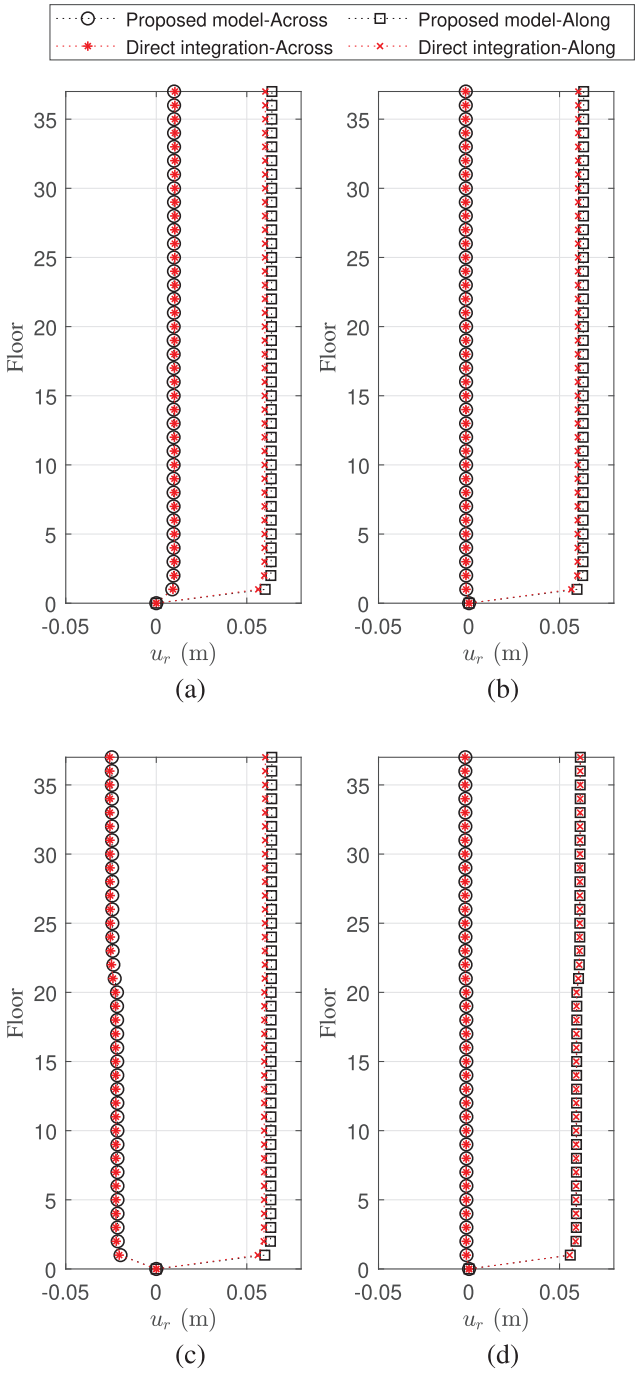

Fig. 6. Comparison between the residual displacements evaluated through the proposed model and direct integration for four randomly selected wind load histories.

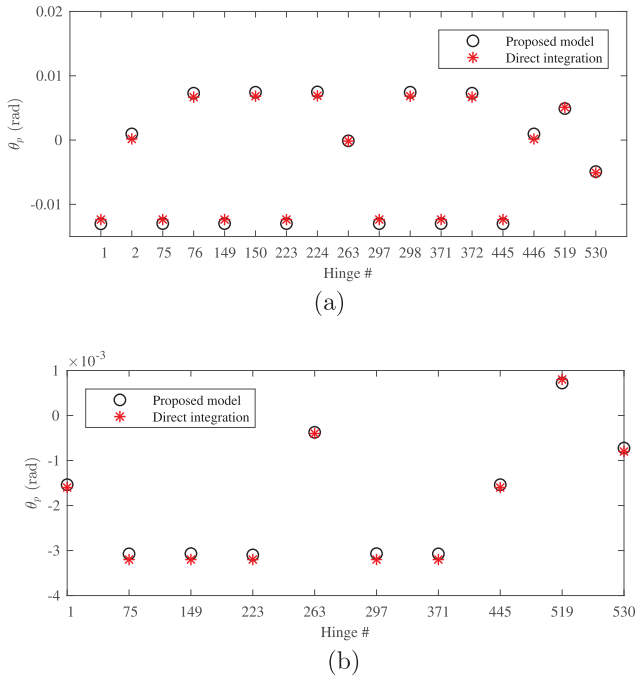

Fig. 7. Plastic hinge rotation, θ_p, for (a) alongwind and (b) acrosswind responses corresponding to the samples generating the residual displacement fields of Fig. 6(a).

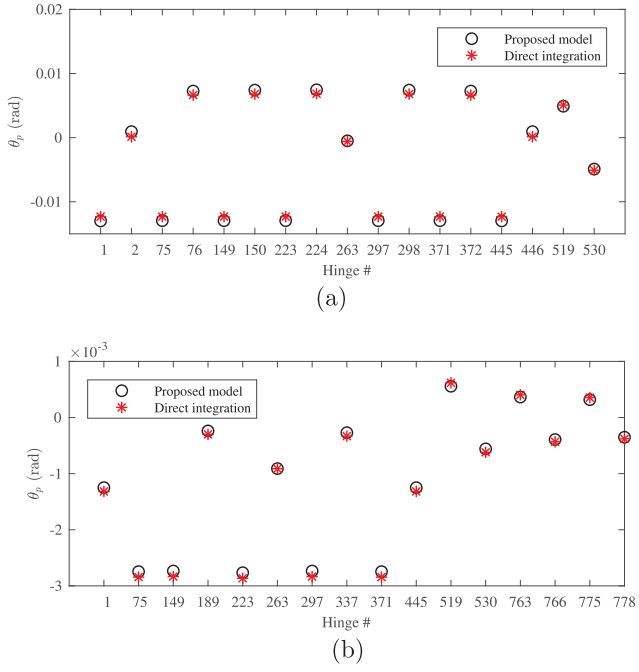

Fig. 8. Plastic hinge rotation, θ_p, for (a) alongwind and (b) acrosswind responses corresponding to the samples generating the residual displacement fields of Fig. 6(b).

alongwind and acrosswind sample generating the residual displacements of Fig. 6(a). In particular, the final residual moments and rotations are marked by squares. As can be seen, after several cycles of loading, an absence of further plastic accumulation is seen as the structure begins to respond in a purely elastic manner, i.e. the state of shakedown has been reached.

Similar results as shown in Figs. 6–8 were seen for the other samples and wind directions. To illustrates this, Fig. 12 shows the comparison between all 200 residual displacements estimated from the strain-based

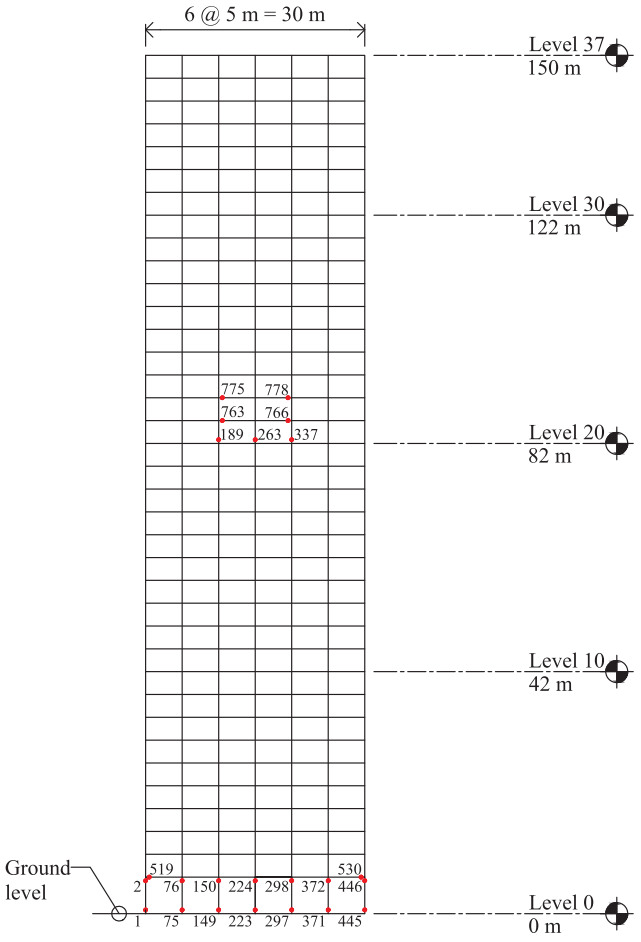

Fig. 9. Plastic hinge locations.

dynamic shakedown scheme and direct integration for the first floor, while Fig. 13 shows the same comparison for the plastic rotations of Hinge 1. As can be seen from these figures, there is strong correspondence between the results of the two methods. Indeed, a correlation coefficient greater than 0.99 existed in both cases. Similar results were seen for all other responses.

Finally, it should be observed that the proposed model estimated solutions for each sample in a matter of seconds while the direct integration approach required around six hours per sample on the same machine. This corresponds to a computational difference of over three orders of magnitude. In particular, it is worth mentioning that the computational efficiency of the proposed model is nearly independent of the length of T (i.e. period of the forcing function). Indeed, this only comes into play in calculating the dynamic steady state elastic response of the system in $[0, T]$, which, due to the elasticity of the system, is negligible. This makes the proposed approach very attractive for systems subject to long duration dynamic loads, i.e. wind excited structural systems.

6.3. Application of the proposed probabilistic framework

In this section, the probabilistic framework of Section 5 is illustrated on the steel frame of Fig. 4. For this application, the wind load histories were given a total length of $T = 3600$ s. A full range of wind directions were considered, namely α was varied between 0° and 90°, for mean wind speeds at the building top of $\bar{v}_y = 52.5$ m/s (approximately 700 year MRI for Miami) and $\bar{v}_y = 56.5$ m/s (approximately 1700 year MRI for Miami). The first five vibration modes with damping ratios of 2.5% were once again considered in estimating the dynamic steady state

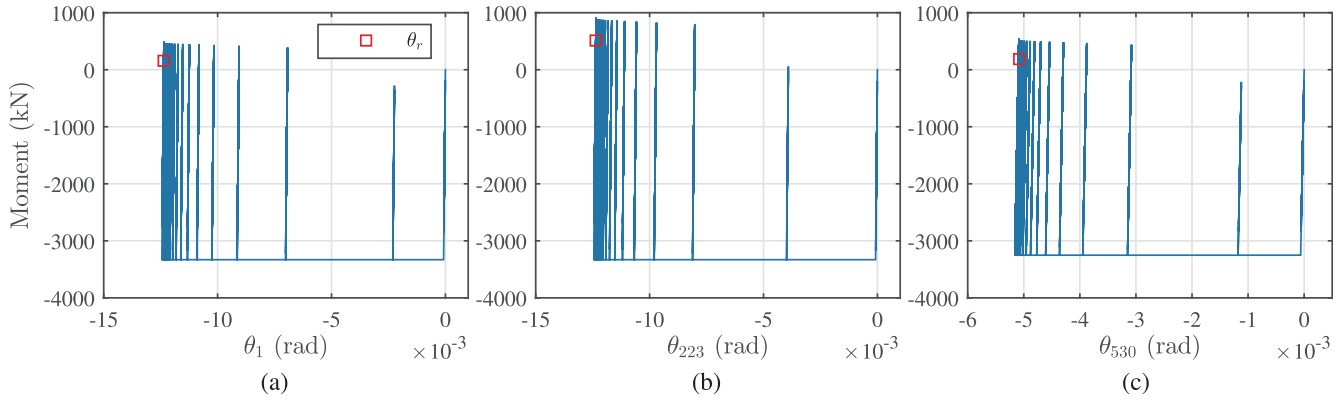

Fig. 10. Moment rotation history corresponding to the sample generating the alongwind residual displacement field of Fig. 6(a) at: (a) Hinge 1; (b) Hinge 223; and (c) Hinge 530.

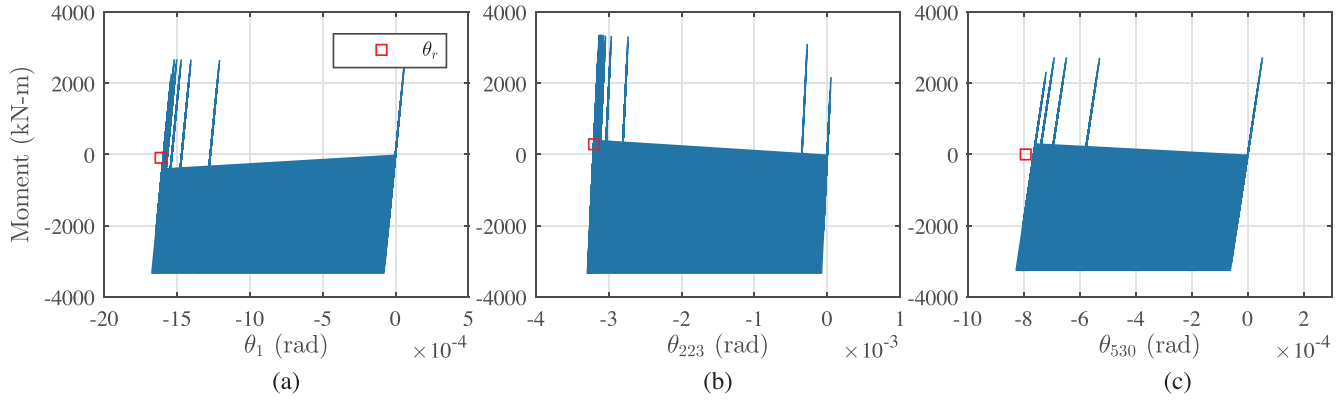

Fig. 11. Moment rotation history corresponding to the sample generating the acrosswind residual displacement field of Fig. 6(a) at: (a) Hinge 1; (b) Hinge 223; and (c) Hinge 530.

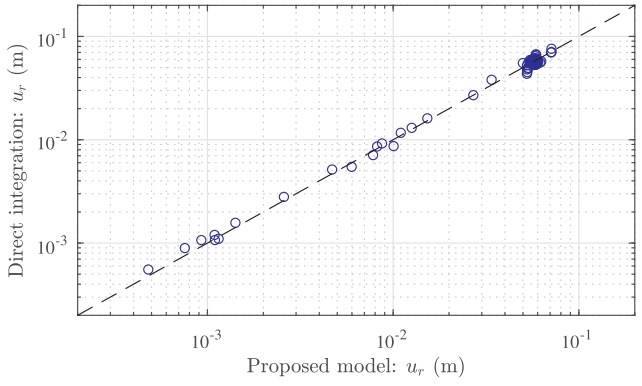

Fig. 12. Comparison between residual displacements at the first floor for all 200 samples.

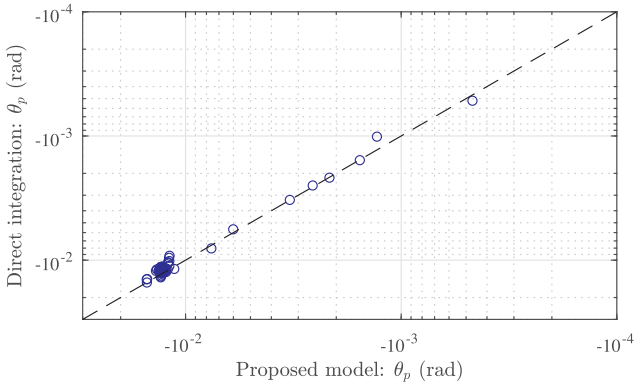

Fig. 13. Comparison between plastic rotations at Hinge 1 for all 200 samples.

elastic response of the system. The following deformation limits were considered for describing failure:

1. Residual drift ratio: $\widetilde{u}_r = 0.5\%$
2. Peak interstory drift ratio: $\widetilde{\widehat{u}}_r = 2.5\%$
3. Plastic hinge rotation: $\widetilde{\theta}_p = 0.01$ rad

These limits were considered for all components of $\mathbf{u}_r$, $\hat{\mathbf{u}}$, and θ_p.

6.3.1. Results

The analyses were carried out for α varying from $\alpha = 0°$ to $\alpha = 90°$ in 10 degree increments and for two wind intensities. For each wind direction and intensity, $N_s = 5000$ samples were considered in the Monte Carlo simulation. Table 2 reports the collapse probabilities for all wind directions and a wind intensity corresponding to an MRI of 700 years while Table 3 reports the analogous quantities for a wind intensity of MRI 1700 years. In particular, as can be seen from Fig. 14, the alongwind ($\alpha = 0°$ in Fig. 4) response of the structural system led to the highest total collapse probabilities. Having said this, in the acrosswind direction ($\alpha = 90°$), the structural system experienced a significant increase in failure probability, with respect to immediately adjacent wind directions, due to vortex shedding. From Tables 2 and 3, it can be seen that, in the alongwind direction, the structure experienced inelastic collapse due to incapability to shakedown, excessive residual drift, and excessive plastic hinge rotations. In the acrosswind direction, on the other hand, failure for this structural system was due exclusively to an incapability to shakedown. For the intermediate wind

Table 2
Inelastic collapse performance for $\bar{v}_y$ with an MRI of 700 years.

Wind direction, α	0°	10°	20°	30°	40°	50°	60°	70°	80°	90°
Non-shakedown collapse prob.	0.0718	0.0534	0.0040	0.0004	0	0	0	0	0	0.0034
Residual drift collapse prob.	0.0474	0.0194	0.0018	0.0002	0	0	0	0	0	0
Plastic hinge collapse prob.	0.0174	0.0098	0.0010	0	0	0	0	0	0	0
Peak drift collapse prob.	0	0	0	0	0	0	0	0	0	0
Total collapse prob.	0.137	0.0826	0.0068	0.0006	0	0	0	0	0	0.0034

Table 3
Inelastic collapse performance for $\bar{v}_y$ with an MRI of 1700 years.

Wind direction, α	0°	10°	20°	30°	40°	50°	60°	70°	80°	90°
Non-shakedown collapse prob.	0.9830	0.9914	0.6372	0.0364	0.0130	0.0064	0.0014	0.0004	0.0488	0.3690
Residual drift collapse prob.	0.0090	0.0022	0.0664	0.0130	0.0050	0.0026	0.0008	0	0.0014	0
Plastic hinge collapse prob.	0.0050	0.0028	0.0506	0.0074	0.0028	0.0020	0.0004	0	0.0018	0
Peak drift collapse prob.	0	0	0	0	0	0	0	0	0	0
Total collapse prob.	0.9970	0.9964	0.7542	0.0568	0.0208	0.0110	0.0003	0.0004	0.0520	0.3690

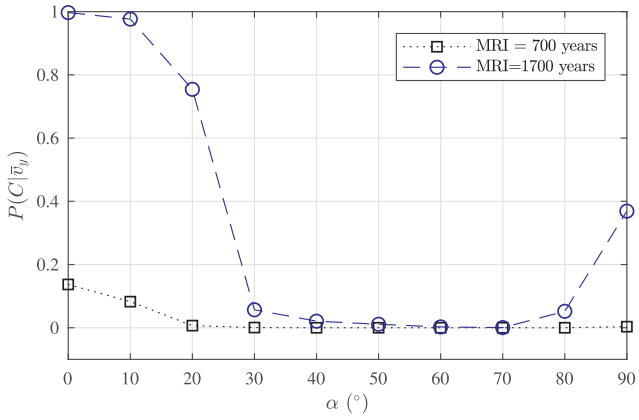

Fig. 14. Variation of the total collapse probability with wind direction.

directions, it is interesting to observe how, for the deformation limits considered in this case study, collapse can easily be produced by excessive deformations. This illustrates the importance of estimating the plastic deformations and strains alongside the shakedown probability in order to fully characterize the collapse of wind excited structural systems. Because the structural system considered in this work showed particular sensitivity to collapse for alongwind and acrosswind actions (the wind directions $\alpha = 10°$ and $\alpha = 20°$ produce, for all intents and purposes, alongwind responses), the following discussion will focus on the wind directions of $\alpha = 0°$ (alongwind) and $\alpha = 90°$ (acrosswind).

As mentioned in Section 5.2, alongside the collapse probabilities, the proposed framework also allows the probability distributions associated with peak/residual deformations and plastic strains at shakedown to be directly estimated. To illustrate this, Figs. 15 and 16 report the exceedance probability distributions associated with the peak horizontal displacement responses given shakedown (*SD*) for the 1st, 20th and 37th floor in the alongwind and acrosswind directions. As can been seen, for low probabilities, significant deviation from the purely elastic peak responses can be observed. As mentioned in Section 2 this information is essential for the correct estimation of $P(DV > dv|NC, im)$ (i.e. losses given that the building does not collapse (*NC*)). Exceedance probability distributions can also be estimated directly in terms of the residual deformations and plastic strains. As an example, Fig. 17 reports the distributions associated with the residual displacements at select floors under 700-year alongwind loads. Fig. 18, on the other hand, illustrates the exceedance probability distributions associated with plastic hinge rotations at two select hinges (see Fig. 9) for 1700-year acrosswind loads. From Fig. 18, it can be observed that for the structure considered in this case study, 57% of Hinge 263 responses, located at the 21st story, experienced plastic deformations while less than 40% of Hinge 223 responses experienced plastic deformations. Through the proposed framework, this kind of detailed information is made available for all 962 possible plastic hinge locations. Similarly, information such as that shown in Fig. 17 is available for all the degrees of freedom

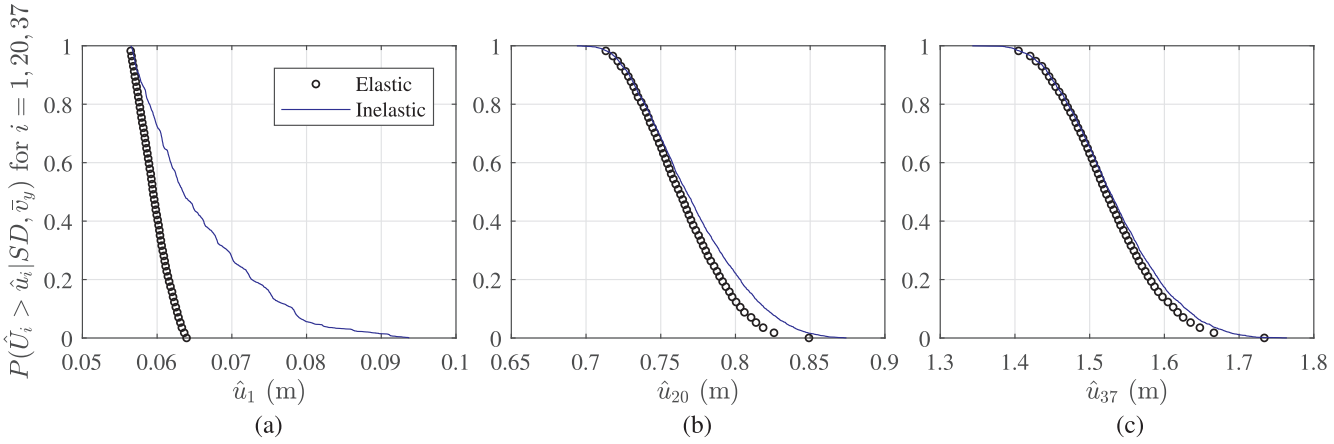

Fig. 15. Probability of exceedance of the alongwind (MRI = 700 years) peak displacement responses at: (a) Floor 1; (b) Floor 20; and (c) Floor 37.

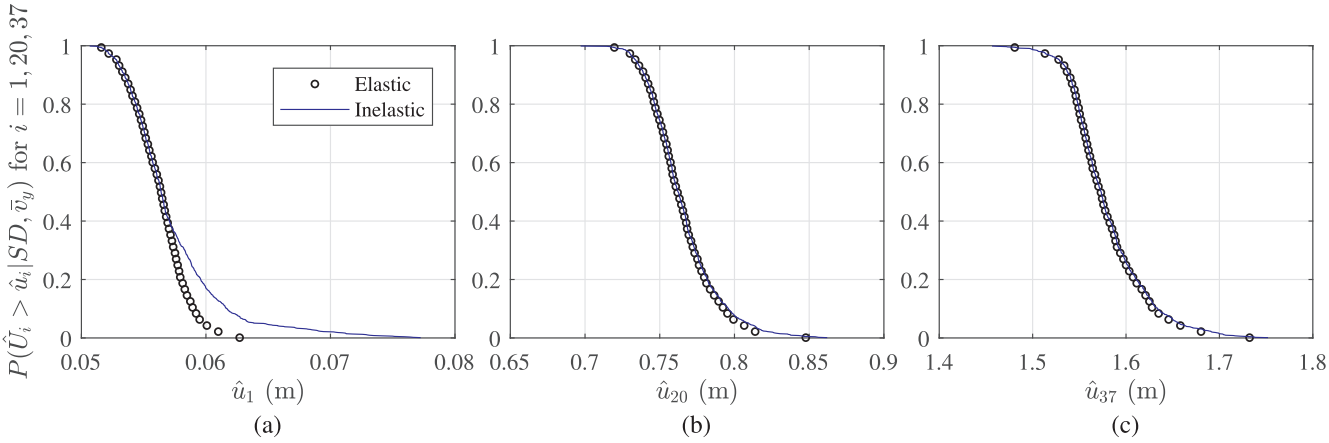

Fig. 16. Probability of exceedance of the acrosswind (MRI = 1700 years) peak displacement responses at; (a) Floor 1; (b) Floor 20; and (c) Floor 37.

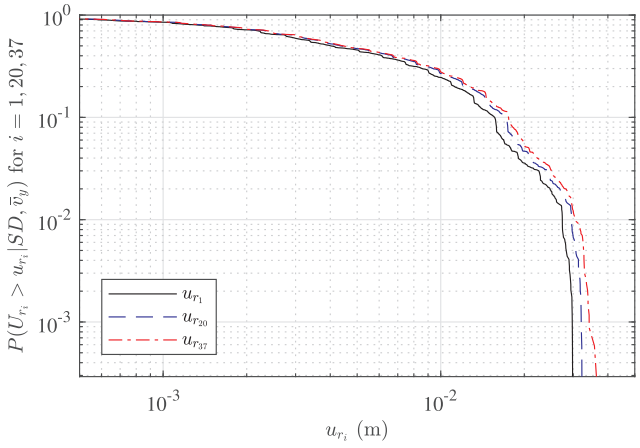

Fig. 17. Probability of exceedance of the residual displacements at Floor 1, 20 and 37 in the alongwind direction with MRI = 700 years.

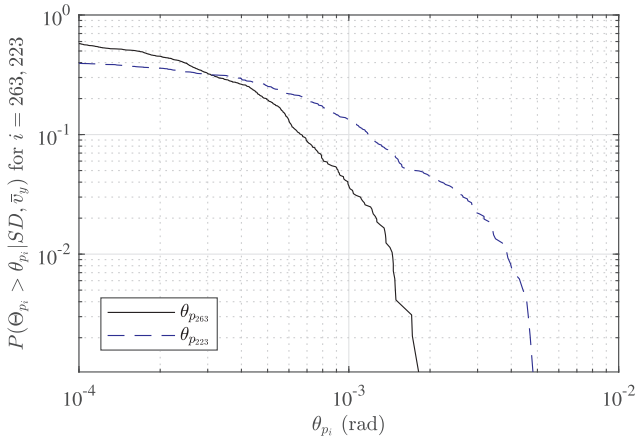

Fig. 18. Probability of exceedance of the plastic hinge rotations for Hinge 263 and Hinge 223 in the acrosswind direction with MRI = 1700 years.

of the system.

Finally, it should be observed that the proposed approach provided the solutions discussed above in a matter of hours. If a similar analysis was carried out by directly integrating the elastoplastic equations of Section 3 for each of the N_s = 5000 samples of the simulation, the estimated run time would be in the order of weeks.

7. Conclusions

The primary objective of the work outlined in this paper was the development of an efficient framework for characterizing the inelastic response of multi-degree-of-freedom wind excited structural systems. Contrary to direct integration approaches, the proposed framework–-which combines classic dynamic shakedown solution methods with a path following strain-based scheme–can estimate the inelastic response at shakedown for a single windstorm in a matter of seconds. This enables the development of simulation-based methods for estimating the probabilities associated with inelastic collapse scenarios involving limit states in terms of plastic deformations and strains occurring at shakedown. A case study consisting of a 37-story steel framework subject to wind tunnel driven stochastic wind loads was presented to demonstrate the potential of the proposed framework. The efficiency and accuracy of the approach was shown, as was the capability to characterize inelastic collapse in terms of modern probabilistic performance-based wind engineering frameworks. In addition, by simulating over a suite of windstorms, the proposed framework is well-suited for identifying critical windstorms for which full step-by-step non-linear analysis could be carried out, therefore providing an exhaustive picture of the inelastic performance of a given wind excited structure.

Acknowledgements

This research effort was supported in part by the National Science Foundation (NSF) under Grant No. CMMI-1462084 and the Magnusson Klemencic Associates (MKA) Foundation under Research Grant Agreement #A101. This support is gratefully acknowledged.

References

[1] NIST. Nonlinear analysis study and development program for performance-based seismic engineering. Tech. Rep.; National Institute of Standards and Technology (NIST); 2013.
[2] Vamvatsikos D, Cornell CA. Incremental dynamic analysis. Earthquake Eng Struc 2002;31(3):491–514.
[3] Ciampoli M, Petrini F, Augusti G. Performance-based wind engineering: towards a general procedure. Struct Saf 2011;33(6):367–78.
[4] Petrini F, Ciampoli M. Performance-based wind design of tall buildings. Struct Infrastruct Eng 2012;8(10):954–66.
[5] Caracoglia L. A stochastic model for examining along-wind loading uncertainty and intervention costs due to wind-induced damage on tall buildings. Eng Struct 2014;78:121–32.
[6] Cui W, Caracoglia L. Simulation and analysis of intervention costs due to wind-induced damage on tall buildings. Eng Struct 2015;87:183–97.
[7] Bernardini E, Spence SMJ, Kwon DK, Kareem A. Performance-based design of high-rise buildings for occupant comfort. J Struct Eng 2015;141(10).
[8] Cui W, Caracoglia L. Exploring hurricane wind speed along US Atlantic Coast in warming climate and effects on predictions of structural damage and intervention costs. Eng Struct 2017;122:209–25.
[9] Chuang WC, Spence SMJ. A performance-based design framework for the integrated

collapse and non-collapse assessment of wind excited buildings. Eng Struct 2017;150:746–58.
[10] Vickery BJ. Wind action on simple yielding structures. J Eng Mech Div 1970;96:107–20.
[11] Tamura Y, Yasui H, Marukawa H. Non-elastic responses of tall steel buildings subjected to across-wind forces. Wind Struct 2001;4(2):147–62.
[12] Hong HP. Accumulation of wind induced damage on bilinear SDOF systems. Wind Struct 2004;7:145–58.
[13] Judd J, Charney F. Inelastic behavior and collapse risk for buildings subjected to wind loads. In: Ingraffea N, Libby M, editors. Structures congress 2015. April 23–25, Portland, Oregon, USA; 2015, p. 2483–96.
[14] Feng C, Chen X. Crosswind response of tall buildings with nonlinear aerodynamic damping and hysteretic restoring force character. J Wind Eng Ind Aerodyn 2017;167:62–74.
[15] Feng C, Chen X. Inelastic responses of wind-excited tall buildings: improved estimation and understanding by statistical linearization approaches. Eng Struct 2018;159:141–54.
[16] Huang MF, Li Q, Chan CM, Lou WJ, Kwok KCS. Performance based design optimization of tall concrete framed structures subject to wind excitations. J Wind Eng Ind Aerodyn 2015;139:70–81.
[17] Krawinkler H, Seneviratna GDPK. Pros and cons of a pushover analysis of seismic performance evaluation. Eng Struct 1998;20(4–6):452–64.
[18] Antoniou S, Pinho R. Advantages and limitations of adaptive and non-adaptive force-based pushover procedures. J Earthquake Eng 2004;8(4):497–522.
[19] Tabbuso P, Spence SMJ, Palizzolo L, Pirrotta A, Kareem A. An efficient framework for the elasto-plastic reliability assessment of uncertain wind excited systems. Struct Saf 2016;58:69–78.
[20] Ceradini G. On shakedown of elastic-plastic solids under dynamic actions. Giornale del Genio Civile 1969;107:239–50.
[21] Corradi L, Maier G. Dynamic non-shakedown theorem for elastic perfectly-plastic continua. J Mech Phys Solids 1974;22:401–13.
[22] Ceradini G. Dynamic shakedown in elastic-plastic bodies. J Eng Mech Div 1980;106:481–99.
[23] Polizzotto C. Dynamic shakedown by modal analysis. Meccanica 1984;19:133–44.
[24] Polizzotto C, Borino G, Caddemi S, Fuschi P. Theorems of restricted dynamic shakedown. Int J Mech Sci 1993;35(9):787–801.
[25] Koiter WT. Shakedown of elastic-plastic structures. North-Holland; 1960.
[26] Federal Emergency Management Agency (FEMA). Seismic performance assessment of buildings, Volume 1 - Methodology (FEMA Publication P-58-1). Washington, DC; 2012.
[27] Federal Emergency Management Agency (FEMA). Seismic performance assessment of buildings, Volume 2 - Implementation (FEMA Publication P-58-2). Washington, DC; 2012.
[28] Federal Emergency Management Agency (FEMA). Seismic performance assessment of buildings, Volume 3 - Supporting electronic materials and background documentation (FEMA Publication P-58-3). Washington, DC; 2012.
[29] Spence SMJ, Kareem A. Performance-based design and optimization of uncertain wind-excited dynamic building systems. Eng Struct 2014;78:133–44.
[30] Maier G. A matrix structural theory of piecewise-linear plasticity with interacting yield planes. Meccanica 1970;7:51–66.
[31] Jirásek M, Bašant ZP. Inelastic analysis of structures. Wiley; 2001.
[32] Cocchetti G, Maier G. Elasticplastic and limit-state analyses of frames with softening plasti-hinge models by mathematical programming. Int J Solids Struct 2003;40:7219–44.
[33] Hachemi A, Weichert D. Numerical shakedown analysis of damaged structures. Comput Methods Appl Mech Eng 1998;160(1–2):57–70.
[34] Simon JW. Direct evaluation of the limit states of engineering structures exhibiting limited, nonlinear kinematical hardening. Int J Plast 2013;42:141–67.
[35] Malena M, Casciaro R. Finite element shakedown analysis of reinforced concrete 3D frames. Comput Struct 2008;86:1176–88.
[36] Comi C, Corigliano A, Maier G. Dynamic analysis of elastoplastic-softening discretized structures. J Eng Mech 1992;118:2352–75.
[37] Mazza F, Mazza M. Nonlinear analysis of spatial framed structures by a lumped plasticity model based on the Haar-Kàrmàn principle. Comput Mech 2010;45:647–64.
[38] Comi C, Corigliano A. Dynamic shakedown in elastoplastic structures with general internal variable constitutive laws. Int J Plasticity 1991;7:679–92.
[39] Casciaro R, Garcea G. An iterative method for shakedown analysis. Comput Methods Appl Mech Eng 2002;191:5761–92.
[40] Palizzolo L, Benfratello S, Tabbuso P. Discrete variable design of frames subjected to seismic actions accounting for element slenderness. Comput Struct 2015;147:147–58.
[41] Chen X, Kareem A. Proper orthogonal decomposition-based modeling, analysis, and simulation of dynamic wind load effects on structures. J Eng Mech 2005;131(4):325–39.
[42] Li Y, Kareem A. Simulation of multivariate nonstationary random processes by FFT. J Eng Mech 1991;117(5):1037–58.
[43] Li Y, Kareem A. Simulation of multivariate random processes: hybrid DFT and digital filtering approach. J Eng Mech 1993;119(5):1078–98.
[44] Li Y, Kareem A. Simulation of multivariate nonstationary random processes: hybrid DFT and digital filting approach. J Eng Mech 1997;123(12):1302–10.
[45] Peng L, Huang G, Chen X, Kareem A. Simulation of multivariate nonstationary random processes: hybrid stochastic wave and proper orthogonal decomposition approach. J Eng Mech 2017;143(9).
[46] Deodatis G. Simulation of ergodic multivariate stochastic processes. J Eng Mech 1996;122(8):778–87.
[47] Bartlett FM, Dexter RJ, Graeser MD, Jelinek JJ, Schmidt BJ, Galambos TV. Updating standard shape material properties database for design and reliability. Research report. American Institute of Steel Construction (AISC); 2001.
[48] AISC. Specification for structural steel buildings. Chicago, IL: American Institute of Steel Construction (AISC); 2010.
[49] Tokyo Polytechnic University (TPU) wind pressure database; 2008. <http://wind.arch.t-kougei.ac.jp/system/eng/contents/code/tpu>.